

Narrow-line external cavity diode laser micro packaging in the NIR and MIR spectral range

A. Jiménez^{1,2}, T. Milde¹, N. Staacke¹, C. Aßmann¹, G. Carpintero², J. Sacher¹

¹ Sacher Lasertechnik GmbH, Rudolf-Breitscheid-Straße 1-5, 35037 Marburg, Germany

² Universidad Carlos III de Madrid, Avenida de la Universidad 30, 28911 Leganés, Madrid, Spain

Received: date / Revised version: date

Abstract Narrow linewidth tunable diode lasers are an important tool for spectroscopic instrumentation. Conventional external cavity diode lasers offer high output power and narrow linewidth. However, most external cavity diode lasers are designed as laboratory instrument and do not allow portability. In comparison, other commonly used lasers, like distributed feedback lasers (DFB) that are capable of driving a hand-held device are limited in power and show linewidths which are not sufficiently narrow for certain applications.

We present new miniaturized types of tunable external cavity diode laser which overcome the drawbacks of conventional external cavity diode lasers and which preserve the advantages of this laser concept. Three different configurations are discussed in this article. The three types of miniaturized external cavity diode laser systems achieve power values of more than 50 mW within the 1.4 μm water vapor absorption band with excellent

side mode suppression and linewidth below 100 kHz. Typical features outstand with respect to other type of laser systems which are of extended use such as DFB laser diodes. The higher output power and the lower linewidth will enable a higher sensitivity and resolution for a wide range of applications.

1 Introduction

New instrumentation tools have been needed to advance in spectroscopy over the last two decades [1]. In this matter tunable lasers have played an essential role, as well as in other sectors such as the medical, pharmaceutical and industrial measurement applications. First generations of diode lasers were composed of large and complex cavities, limiting the use of these devices only to controlled laboratory environments. Some methods can also be applied to narrow the linewidth of semiconductor lasers,

such as locking the emission wavelength to an external Fabry-Perot cavity [2], but this method implies adding complexity to the tunable laser diode systems. Thanks to research in assembly technologies, these drawbacks are beginning to be overcome in systems which are more robust and environmentally insensitive. However, the high costs of diode laser systems still represent a limitation for their use in general applications. This article discusses recent technology advancements which allow significant improvements in terms of packaging and integration of tunable and highly stable laser solutions.

Section 2 will describe the three main architectures discussed in this article, which are three different approaches for micro external cavity lasers. The first approach includes a Volume Holographic Grating (VHG) as a feedback element, the second approach employs a state of the art micro Littman-Metcalf cavity structure in a miniaturized version and the third device relies on a transmission grating and a tunable Micro Electro Mechanical System (MEMS) to create the external cavity. Each of the solutions offers promising operation parameters in terms of power and linewidth of the developed devices while reducing the size for portable and handheld operation. Recently, progress has been made in the direction of miniaturizing tunable laser diode systems, as devices have been reported in a miniaturized VHG setup from Luvsandamdin et al. [3]. Also MEMS actuated tunable devices have been reported with the use

of reflection gratings by Berger et al. [4] and later by Huang and Cai [5,6].

In the third section, results are shown for absorption and photoacoustic spectroscopy applications and later a discussion is established on the main advantages of this kind of micro integrated external cavity diode lasers.

2 External cavity configuration

2.1 Volume Holographic Grating

Independently from the final support in which the device is going to be mounted (mainly butterfly package or TO can), the diode gain chip is mounted on a copper tungsten microbench together with the rest of the necessary parts of the laser systems setup. The system is composed of a ridge waveguide emitting (RWE) laser, fast and slow axis collimating lenses and a VHG. The RWE laser chip can also feature an angled output for enhanced operation. The laser diode (LD) chip is composed of a multiple quantum well InGaAsP ridge waveguide. The semiconductor material is soldered and bonded on an AlN submount for good heat dissipation, which in turn is placed on the copper tungsten micro-bench with the rest of the elements that form the laser system. The whole laser is temperature stabilized near room temperature. Aspherical cylindrical lenses have been used to collimate the laser. The material of these lenses is Lanthanum flint (N-LaF21) with focal lengths of 1.0 mm and 2.1 mm for the fast and slow axis respectively. The numerical aper-

ture (NA) is 0.8 for the Fast Axis Collimation (FAC) and 0.11 for the Slow Axis Collimation (SAC) and both have an anti-reflection (AR) coating with $R < 0.5\%$. The resonator is formed between the rear side of the laser diode with a high reflection (HR) coating, $R > 95\%$, and the end of a transmitting VHG recorded in photo-thermo-refractive glass (PTR-glass). To avoid undesired feedback effects from the front facet of the diode, an AR coating of $R < 0.1\%$ was used. The VHG has been employed as high efficiency, low loss intracavity filter in order to achieve a high beam quality. The AR coated VHG, which is placed at a distance of 5 mm from the LD, is centered around the wavelength of interest and reflects 10% of the incoming intensity back into the LD. This value was selected to optimize the output power of the device as it is later discussed in Section 3. The length of the VHG will vary depending on the wavelength of interest to achieve the specified feedback level. Figure 1 shows a Computer Assisted Design (CAD) model of the VHG laser system within a standard butterfly package.

This concept allows an improved performance of the laser diode system. The output power is in excess of 50 mW for the wavelength range described in this system ($\lambda = 1396\text{nm}$) although it can go up to 350 mW in the 780nm wavelength range [7], being the side mode suppression ratio (SMSR) typically 50 dB or better and linewidth values below 100 kHz due to the extremely good selectivity of the Bragg grating. The accuracy in the fabrication of the gratings [8] allows the option of ad-

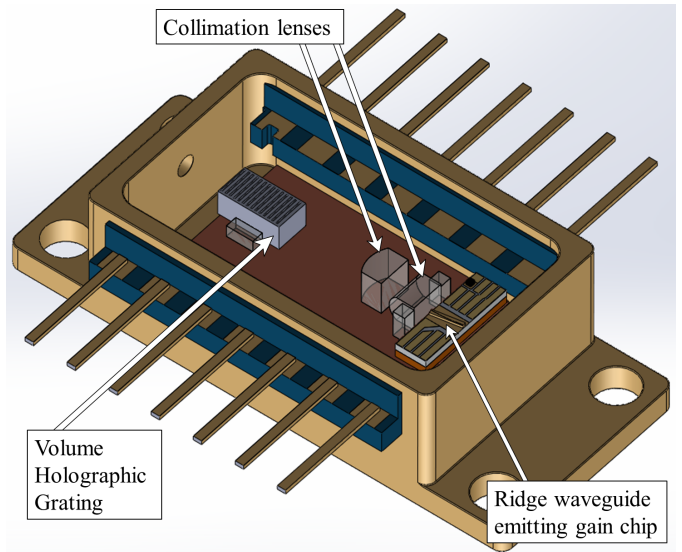


Fig. 1 CAD model of the developed VHG laser system. The system is composed of a RWE gain chip, collimation lenses and a spectrally selective VHG to close the cavity.

ressing this concept to any wavelength region, offering an incredible freedom to specifically target any particular wavelength of interest.

The tuning for these VHG laser systems is achieved by varying the injection current of the laser diode chip. Tuning ranges of up to 20 GHz can be reached.

2.2 Micro Littman-Metcalf

Although the Littman-Metcalf laser cavity is already known and is extensively used for tunable laser systems, the external cavity normally leads to complex setups which cannot be reduced in size due to the mechanical layout. Hence, the main improvement point is the reduction of the size of these systems to enable compact sized measuring instruments and portability. We demonstrate here the ability to integrate such a complex cavity

in a butterfly type case, which allows a reduced system size without compromising the laser operating characteristics.

Figure 2 shows the schematic view of a Littman-Metcalf external cavity laser. An angled RWE chip is used on AlN substrate, which is mounted on a micro-bench so that the two sides of the gain chip will be accessible. The chip is coated to tune the performance of the laser diode system. On the cavity side, an AR coating with $R < 0.1\%$ is applied, while on the output side the coating is adjusted to match $R \simeq 20\%$ because the high reflectivity is already provided by a silver mirror which closes the cavity. This parameter is later discussed in Section 3. On the right part of the diode chip an aspherical lens is used for collimating the diode's AR output before being shined on a reflection grating. The lens used has a NA of 0.60 and a focal length of 2.80 mm. The AR coating of the lens will be matched to the emission wavelength of the corresponding laser diode, which in the case of a 1396nm system, will be coated with $R < 0.25\%$ for the wavelength range between 1300 nm and 1600 nm. The reflection grating, with 900 lines/mm, acts as an intra-cavity filter which will select the lasing mode from the gain chip, while the silver mirror will feed back the zero order reflection from the reflection grating to close the cavity with the rear facet of the diode to lase in a stable mode.

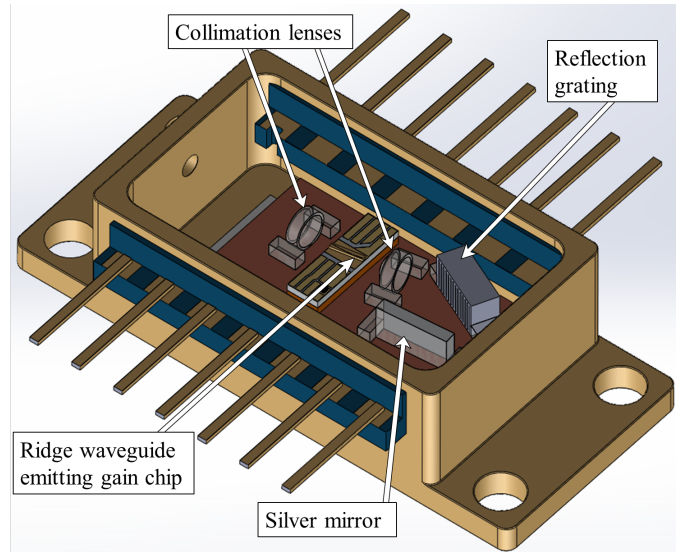


Fig. 2 CAD model of the developed Micro Littman-Metcalf laser system. The system is composed of an angled RWE gain chip, collimation lenses in the cavity and output sides, a reflection diffraction grating and a silver mirror.

When the device is being assembled, the mirror can be tilted to select the central wavelength in an extremely precise way to address the desired frequency. Once all the elements are fixed, the device can still be slightly tuned over current, allowing a scan in the GHz range which can be applied for a variety of applications. Some of these will be discussed in this article.

The output of the laser is taken at the straight output of the diode chip with the same lens that is used in the cavity side, which has an easy access at the side of the microbench in order to collimate the output beam as well as the beam employed to generate the cavity. By using this two-sided approach instead of outcoupling the light via the first order of the grating, the system has a series of advantages: polarization ratios over 1:200, SMSR

with values over 60 dB and no beam walk at the output of the laser [9]. An increase of the output power and the beam quality of the Littman-Metcalf laser is achieved by using a high efficiency grating. The narrowband selectivity of the grating ensures the single longitudinal mode operation.

One of the further advantages of having an operationally independent output is that the collimation of the output beam can be tuned for the desired application while the collimation inside the resonator is optimized for best illumination of the grating. The system can even be employed for high power tapered laser diodes within a Littman-Metcalf configuration with output powers of over 2500 mW. This would allow the replacement of common master-slave laser systems within extremely compact and portable devices.

The advantages of this system combine a high frequency stability together with a small linewidth and maximum output power. The resonator quality ensures high side mode suppression ratios.

2.3 Transmission grating design

One of the key points of this design is to expand the tuning range of the laser system without compromising the size. The reflection grating is replaced by a transmission grating. A CAD model of the developed setup with the transmission grating is shown in Figure 3.

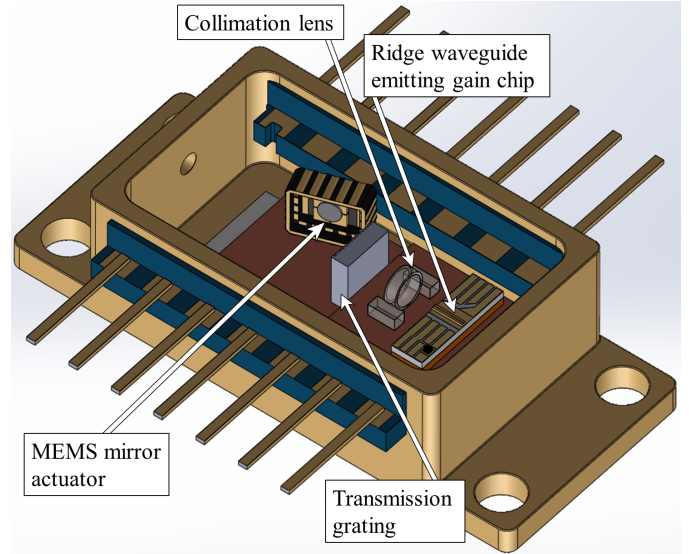


Fig. 3 CAD model of the developed micro transmission grating laser system. The system is composed of a RWE gain chip, a collimation lens, a transmission diffraction grating and a MEMS actuator containing a tilting mirror which closes the cavity and allows a broad tuning range.

In this setup, the grating also acts as an intra-cavity filter, but the mirror is replaced by a Micro Electro Mechanical System (MEMS) actuator, which will enable the option of tilting the reflected beam in order to tune the wavelength. The whole device can be still mounted in a very compact package without any compromise in the performance of the laser. Furthermore, it broadly extends the tuning range of the device over the whole gain bandwidth of the laser chip. A RWE gain chip is also used in the setup. Its rear facet is HR coated ($R > 95\%$) and its front facet is AR coated with $R < 0.1\%$. The lens used in this setup is the same as in the micro Littman setup ($NA = 0.6$, $F = 2.8\text{mm}$) and is AR coated with $R < 0.25\%$. The transmission grating has 1200 lines/mm

and is AR coated on its back plane to avoid undesired reflections from the surface.

Concerning the MEMS, it is composed of a one dimensional tilting mirror which allows the option of tuning the device. The beam from the laser is collimated with the aforementioned aspherical lens and then shined into the transmission grating. The beam goes through the grating and is diffracted in the rear facet that contains the grooves. The beam is then broadened according to a spatial distribution of the laser's emitted wavelengths. The system can be tuned thanks to the variable tilt angle of the MEMS mirror. The mirror actuator, which can be tilted up to $\pm 5^\circ$, has a round shape and its diameter is 2mm . It is also HR coated, improving the efficiency of the cavity by means of reducing the losses in the reflection. In order to protect the MEMS actuator, a window covers the device on its package, and this element is AR coated to avoid undesired effects in the cavity, which is finally formed between the HR coated rear facet of the laser diode chip and the MEMS actuator mirror.

This technology can be applied to any wavelength of interest by the appropriate selection of the system's elements. Figure 4 shows the tunability of a 780 nm centered diode, achieving a tuning range of more than 40 nm and a maximum output power of 67.3 mW.

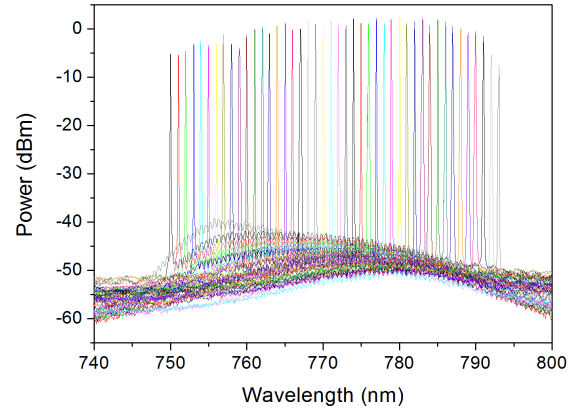


Fig. 4 Optical emission spectrum of the tunable transmission grating laser. The system is demonstrated to tune over a span of $> 40\text{nm}$ around the center wavelength of 780nm with a peak power of 67.3 mW.

3 Applications

Within the wide variety of fields in which compact laser systems can be employed, some of them are especially important nowadays for research and industry applications. The different lasers which have been presented in this article enable very compact devices for measuring systems, enabling even hand-held type of Raman spectrometers due to the high power provided.

In this publication the focus will be made on gas detection. Different techniques can be driven with help of laser systems, among which absorption and photoacoustic spectroscopy are of special importance [10]. Two experiments are presented regarding these two measuring methods.

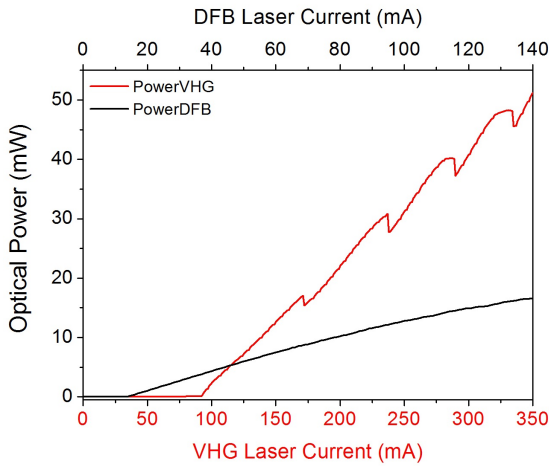


Fig. 5 The output power of a VHG and a DFB laser are compared. The VHG *red* generates an output power of 51.2 mW while the DFB *black* is limited to 16.6 mW .

3.1 Absorption spectroscopy

This kind of spectroscopy measures the absorption of laser intensity when the laser beam is shined through a gas sample. The gas will absorb energy at a specific wavelength depending on the gas and other parameters such as concentration, pressure or temperature.

An experimental setup with a VHG laser system was used to detect water vapor. The VHG is in the region of 1397 nm, where a strong water vapor absorption line is present. The laser system is composed of a ridge waveguide emitting laser, fast and slow axis collimating lenses and a VHG. Figure 5 shows the Power vs. Current performance of a VHG laser compared to a DFB in the 1390 nm range at a temperature of 20°.

Two main effects can be observed in this graph. The first one is related to the small kinks present in the VHG curve (red line in Figure 5), and the second effect re-

fers to the increased threshold current and output power which the VHG laser systems exhibit. The power variations through the VHG power curve correspond to changes in the lasing mode which is stabilized in the cavity. The mode which lases in the cavity is swept due to the increasing current in the laser chip throughout the pass band of the volume holographic grating. When the lasing mode reaches the higher edge of the VHG spectral band, another mode begins to lase in the lower wavelength of the VHG band and becoming dominant. This behavior is repeated several times through the current scan as it will be shown in Figure 8, at the end of this section.

In order to analyze the increased threshold current and output power which the VHG laser systems show, one main effect needs to be taken into consideration: the reflectivity needed for a proper single mode operation. For DFB waveguide gratings, a higher spectral selectivity causes higher losses due to a strong overlap of the optical lasing mode with the DFB grating inside the waveguide. This is opposite to VHG lasers, which allow increasing the spectral selectivity almost without increasing the losses. Hence, it is possible to increase the chip length compared to DFB lasers and therefore also inject a higher current to the devices. The requirement for a narrower spectral selectivity for proper single mode operation can be achieved with a narrower selectivity of the VHG without significantly higher losses. Furthermore, the power of the VHG laser can be further increased by

a lower reflectivity of the grating. These combined changes compared to a DFB laser result into a significantly higher optical power output, as well as into a higher threshold current. The main contribution for these effects comes from the reflectivity of the cavity mirrors, which induces a change in the feedback level of the laser diode resulting in changes in the threshold current and final output powers [11, 12]. The losses in the mirrors are modeled by Equation 1:

$$k_r = \frac{1}{L} \ln\left(\frac{1}{\sqrt{R_1 R_2}}\right) \quad (1)$$

where k_r corresponds to the mirror induced losses depending on L , the chip length, and on the facet reflectivities of the facet. This losses modify the threshold current, which can be derived from the threshold current density J_{th} that is described in Equation 2:

$$J_{th} = J_0 + \beta^{-1} k_r \quad (2)$$

being β the gain constant and J_0 the linear extrapolation term [13]. These effects have a final impact on the output power available at the output of the laser system as stated in Equation 3, which explains the existence of a maximum on the $P_{out}(R_2)$ curve relating the output power with the reflectivity of the output facet:

$$P_{out} = \frac{h\nu_{las}}{q} \eta_{int} (I - I_{th}) \frac{k_r}{k_r + \rho} \quad (3)$$

Here h is Planck's constant, ν_{las} is the laser's frequency, q is the electron's charge, η_{int} represents the

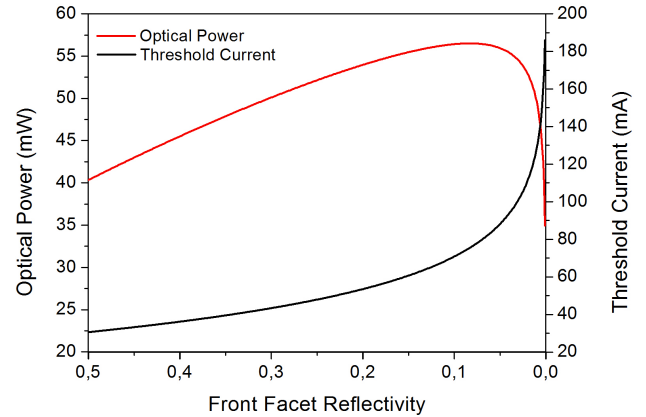


Fig. 6 Output power and threshold current simulation of a laser diode vs the front facet reflectivity. The optical power, *red*, shows its maximum value for a reflectivity of 8.3% while the threshold current, *black*, follows an exponential increase as the front facet reflectivity is decreased.

internal efficiency of the laser and ρ describes the internal optical loss of the device. Figure 6 represents the behavior of the VHG setup described in Section 2.1. It can be seen that the threshold current and the optical power from the laser system depend on the chosen reflectivity for the front facet. The threshold current shows an exponential increase which is described in Equation 2, and the optical power can be maximized by tuning R . The value which has been chosen is $R = 10\%$, which maximizes the output power while keeping a moderate lasing threshold. When comparing the VHG values to DFB devices (Figure 5), the latter possess a higher reflectivity because of the waveguide grating which ensures single mode operation. This fact leads to a decrease in the threshold current.

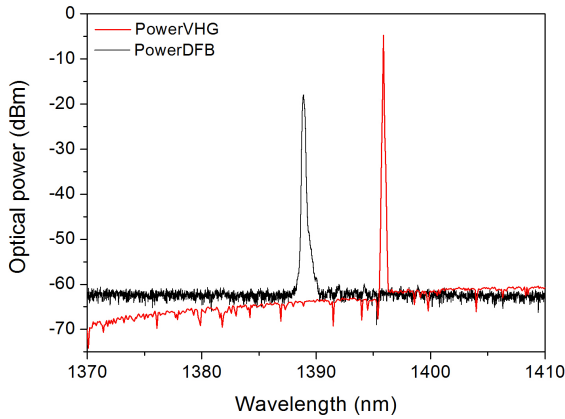


Fig. 7 Optical spectrum of a VHG *red* and a DFB laser *black*. The SMSR of the VHG results in a value of 55.91 dB, compared to the SMSR of 41.92 dB of the DFB laser.

In addition, the spectrum of the ECDL compared to the one of the DFB laser is shown in Figure 7. The Side Mode Suppression Ratio (SMSR) of the VHG laser is of 55.91 dB while the one exhibited by the DFB laser is of 41.92 dB. This means a difference of more than 10 dB in favor of the VHG laser. An output power in excess of than 50 mW is achieved in the 1.4 μm range for the VHG laser, with a SMSR higher than 55 dB and a total tuning span of over 7 GHz.

VHG lasers receive optical feedback from a high quality holographic grating, which is comparable to the normal facet reflectivity of laser diode chips. Therefore, the losses are not significant with respect to the ones introduced by the grating present in DFB laser diodes, where the interaction of the grating and the waveguide reduces the output power of the devices. This is the reason why VHG lasers show significantly higher output power.

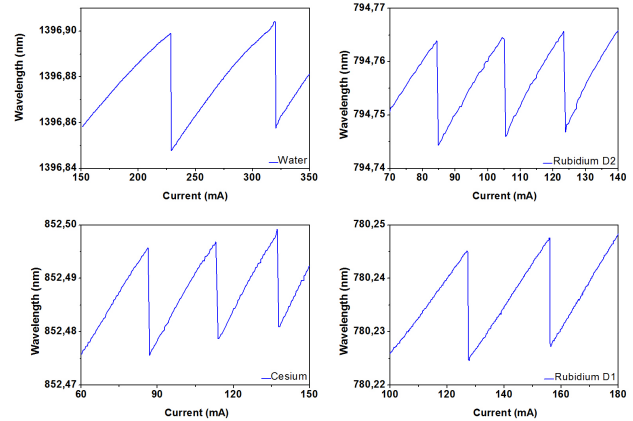


Fig. 8 Wavelength tuning of different VHG systems addressing four different gas absorption lines: Water vapor (*upper-left*), Cesium (*bottom-left*), Rubidium D1 (*upper-right*) and Rubidium D2 (*bottom-right*).

By means of stabilization of the VHG laser at a specific temperature, the exact line of absorption of water vapor of 1396.6 nm can be addressed. In addition, the linewidth of a VHG laser was calculated by beating two identical systems. Due to the high stability both in long term and short term, no external locking was needed to stabilize the two laser systems. Two beating laser modes at 1 ms sweep time from identical lasers, were fitted with a Lorentzian signal. The optical linewidth of the system is estimated to be lower than 20 kHz at the Full Width Half Maximum (FWHM). Among the main advantages of this system is the addressing to any wavelength of interest with high precision. Different wavelength VHG systems have been experimentally tested and are shown in Figure 8.

3.2 Photoacoustic spectroscopy

Photoacoustic spectroscopy is nowadays becoming of special importance in the field of gas trace detection [14, 15]. This offset-free technique enables the possibility of more precise measurements. Among the photoacoustic gas trace detection methods [16], it is necessary to mention QEPAS (Quartz-Enhanced Photoacoustic Spectroscopy)

This approach to photoacoustic detection of gases employs a quartz tuning fork (QTF) to resonantly detect weak photoacoustic signals even with very small concentrations of the target gas samples [17–19]. A quartz crystal is used due its low loss and low cost, being a mature technology used for a long time in daily used devices such as clocks or common electronic devices.

Usually, QTFs have a resonant frequency of approximately 32,768 Hz and provides a quality resonance factor between 10,000 and 100,000 depending on the pressure conditions. QTFs are quadripoles, providing good environmental noise immunity for external acoustic sources. The way to drive this QEPAS detector is to make the laser beam pass through the gap between the two prongs of the tuning fork without touching them.

A setup was made to detect methane with a QEPAS cell from TU Clausthal [17,20]. In order to compare the results from this experiment, the absorption spectra of methane was also measured. While the absorption spectroscopy was limited in terms of detection, the QEPAS photoacoustic method employed was still

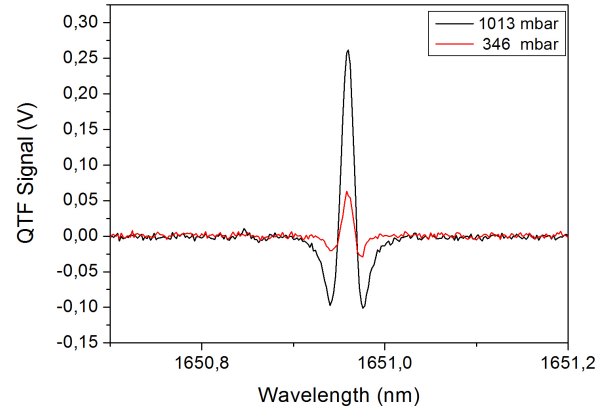


Fig. 9 Photoacoustic signal of methane measured in the QTF of a QEPAS cell for pressures of 1013 mbar (*black*) and 346 mbar (*red*) with an optical power of 25 mW.

able to detect a low volume of gas within the QEPAS cell. Figure 9 shows the detected signal of methane absorption for two different pressures measured in the cell: 1013 mbar and 346 mbar.

Another important factor to take into account is that the signal is proportional to the received power, as stated in Equation 4 [19]:

$$S \propto \frac{Q \cdot P \cdot \alpha}{f_0} \quad (4)$$

where S refers to the measured photoacoustic signal, Q is the quality factor of the acoustic resonance of the tuning fork, P is the laser power, α is the absorption coefficient of the gas trace and f_0 corresponds to the resonant frequency of the QTF present in the QEPAS cell.

This is experimentally demonstrated in Figure 10, where two different power levels have been employed

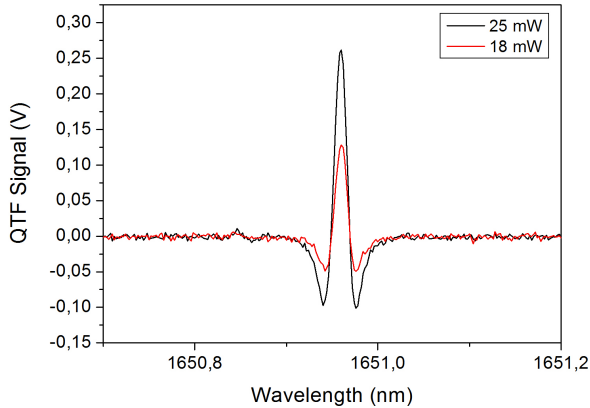


Fig. 10 Photoacoustic signal of methane measured in the QTF of a QEPAS cell for 18 mW (*red*) and 25 mW (*black*) laser output power, showing an increase in the measured fork signal. The pressure in the QEPAS cell is of 1013 mbar.

to detect the same gas concentration within the QEPAS cell. With a higher power level (25 mW compared to 18 mW), the detected signal increased in relation to the present noise, offering an increased SNR which was measured up to 28.58 dB. Hence, the sensitivity of the measuring system is increased with the presented devices due to a higher output power. With the absorption spectroscopy setup, methane could be detected at atmospheric pressure (1013 mbar), but no signal was present when the pressure was decreased to 346 mbar. These results reinforce the use of QEPAS, which has been demonstrated to increase the sensitivity of the measurement system even at the lowest power employed.

4 Results and discussion

We demonstrate the suitability of our new high power compact tunable laser systems with three different concepts for spectroscopic applications. Each of these concepts can be addressed to any wavelength within the available gain chip laser diodes reaching high power and narrow linewidth. All the systems are integrated within compact cases (i.e. butterfly package) enabling portability and hand-held operated instruments. In this section, our research is reported in terms of the most important characteristics to boost the sensitivity and the resolution of spectroscopy systems. Furthermore, we performed a high resolution photoacoustic spectroscopy (QEPAS) experiment which shows the excellent suitability of such high power and narrow linewidth lasers for this kind of application.

4.1 Power characteristic

In order to provide high output power, the ECDL systems presented in this article make use of Fabry-Perot diodes with an antireflection coating in the cavity facet. This coating, in the order of 10^{-4} to 10^{-5} is necessary to prevent mode competition between the internal diode modes and the external resonator modes. Furthermore, the reflectivity parameters of both ends of the cavity are tuned to obtain optimum performance and maximum power as it was discussed in Section 3.1.

The laser systems which have been presented exhibit a big difference in power with commercially available systems usually employed for spectroscopy applications like DFB laser diodes. A typical value of power for commercial diodes near the water absorption spectrum at 1396 nm would be 5 mW. In comparison, the laser systems shown here have been proven to deliver over 50 mW of output power, which was shown in Figures 5 and 6, due to the reduced losses in the cavity.

4.2 Linewidth

The linewidth of an ECDL is mainly determined by the injection current noise of the laser driver and by mechanical vibrations. Thanks to the monolithic approach of the presented laser systems, mechanical vibrations are greatly reduced compared to a more complex and bulky cavity. When performing high resolution spectroscopy measurements, a narrow linewidth of the laser source is essential. To keep the linewidth as narrow as possible, an ultra-low-noise laser diode driver was used with the ECDL laser systems. The linewidth of the VHG system was then measured via a heterodyne experiment of two VHG systems.

Figure 11 shows the beat signal of two identical VHG systems. The measurement was linearized to determine the FWHM linewidth with a Lorentz fit. Taking into account that the value is the result of the beat signal of two similar systems, the optical linewidth was measured to be of 18 kHz, which clearly demonstrates the excellent

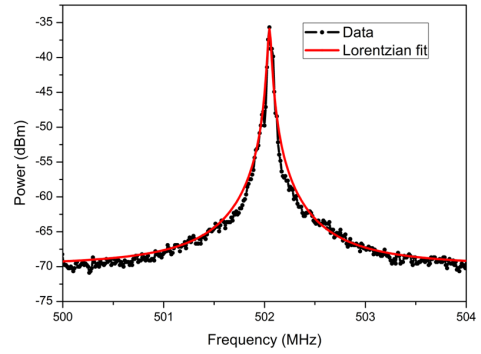


Fig. 11 Heterodyne linewidth measurement of two identical VHG systems. The Lorentzian fitted signal shows an optical linewidth value of 18 kHz for the laser system.

performance of the system in terms of narrow linewidth. This result can be compared to the ones presented by Luvsandamdin [3], where a measured FWHM linewidth of 47 kHz was reported.

4.3 Spectroscopic application

The suitability of these laser systems for spectroscopic applications was demonstrated throughout two experiments: absorption and quartz-enhanced photoacoustic spectroscopy. Different laser wavelengths were shown addressing different gases absorption spectrums: water vapor, oxygen, cesium and rubidium (Figure 8). With this very precise setting of the wavelength, the laser wavelength can be swept around the desired absorption line of the chosen gas. Locking techniques can be applied to these laser systems thanks to a high speed bias tee included in the presented devices for applications such as atom trapping and cooling.

The laser source, together with a QEPAS cell, was also proved to work with a photoacoustic spectroscopy setup to detect methane at a wavelength of 1651 nm. In this region, methane presents a strong absorption line. For the spectroscopy experiment, the QEPAS cell was filled with methane gas and the flow rate was controlled by an electronic mass-flow controller at a temperature of 294 K and a pressure of 1013 mbar. Two different laser beam power levels were employed to measure the photoacoustic signal generated by the fork of the QEPAS cell. For the first power level, 18 mW, the signal to noise ratio of the measurement was calculated to be 13.04 dB. With the second power level, 25 mW, the signal to noise ratio increased up to 28.58 dB.

The presented data is in agreement with the fact that the signal is proportional to the optical power which passes through the fork of the QEPAS cell, which means that a higher power yields an increased SNR and therefore a higher sensitivity.

5 Conclusions

We reported on a new technology of micro integration for high power laser diodes in different external cavity configurations. These designs offer a high output power which is scalable to any wavelength of interest. The laser systems offer a narrow linewidth below 20 kHz within a compact package which enables portability and handheld device operation. We also demonstrated the suitability of the system for absorption and quartz-enhanced

photoacoustic spectroscopy in a gas detection experiment. The high output power of the laser systems yields an increase in the signal to noise ratio allowing a higher sensitivity of the experiment. This study is a proof of the high potential of the micro integrated ECDL systems as a cost effective solution.

6 Acknowledgments

We gratefully acknowledge the German Federal Ministry of Education and Research (BMBF) for the support of our research in the project *CheqVAP*, grant identifier No. 13N13402 and in the project *PhotoBiosense*, grant identifier No. 13N1382. Within this project the quartz enhanced photoacoustic experiments were done at the Institute for Energy Research and Physical Technologies at Clausthal University of Technology. For performing these measurements we specially thank Mario Mordmüller.

References

1. C. E. Wieman, L. Hollberg: Review of Scientific Instruments **62**, **1** (1991) 1-20.
2. W. Lewoczko-Adamczyk, C. Pyrlik, J. Hger, S. Schwertfeger, A. Wicht, A. Peters, G. Erbert, G. Trnkle: Opt. Express **23** (2015) 9705-9709.
3. E. Luvsandamdin, S. Spießberger, M. Schiemangk, A. Sahm, G. Mura, A. Wicht, A. Peters, G. Erbert, G. Tränkle: Appl. Phys. B **111** (2013) 255260.
4. J. D. Berger, Y. Zhang, J. D. Grade, H. Lee, S. Hrinya, H. Jerman, A. Fennema, A. Tselikov, D. Anthon: Proc. 27th

- European Conference on Optical Communications **2** (2001) 198-199.
5. W. Huang, R.R.A. Syms, J. Stagg, A. Lohmann: IEE Proceedings - Science, Measurement and Technology **151**, **2** (2004) 67-75.
 6. H. Cai, X. M. Zhang, J. Wu, D. Y. Tang, Q. X. Zhang, A. Q. Liu: Transducers 2007 - 2007 International Solid-State Sensors, Actuators and Microsystems Conference (2007) 1433-1436.
 7. S. Rauch, J. Sacher: IEEE Photonics Technology Letters **27**, **16** (2015) 1737-1740.
 8. B. Jacobsson, V. Pasiskevicius, F. Laurell, V. Smirnov, L. Glebov: Conference on Lasers and Electro-Optics/Quantum Electronics and Laser Science Conference and Photonic Applications Systems Technologies (2008) CTuY3.
 9. S. Stry, S. Thelen, J. Sacher, D. Halmer, P. Hering, M. Mrtz: Applied Physics B **85**, **2** (2006) 365-374.
 10. A. Elia, P.M. Lugarà, C. Di Franco, V. Spagnolo: Sensors **9** (2009) 9616-9628.
 11. J. Sacher, D. Baums, P. Panknin, W. Elsässer, E. O. Göbel: Physical Review A **45**, **3** (1992) 1893-1905.
 12. L. Hildebrandt, R. Knispel, S. Stry, J. R. Sacher, F. Schael: Applied Optics **42**, **12** (2003) 2110-2118.
 13. V. P. Gribkovskii: Progress in Quantum Electronics **19** (1995) 41-88.
 14. F. K. Tittel, R. Lewicki, M. Jahjah, Y. Ma, P. Stefan-ski: 2012 Asia Communications and Photonics Conference (ACP) (2012) 1-1.
 15. L. Dong, J. Wright, B. Peters, B.A. Ferguson, F.K. Tittel, S. McWhorter: Applied Physics B **107** (2012) 459-467.
 16. A.A. Kosterev, L. Dong, D. Thomazy, F.K. Tittel, S. Overby: Applied Physics B **101** (2010) 649-659.
 17. A.A. Kosterev, Y.A. Bakhirkin, R.F. Curl, F.K. Tittel: Opt. Lett. **27** (2002) 1902-1904.
 18. A.A. Kosterev, F.K. Tittel, D. Serebryakov, A. Malinovsky, A. Morozov: Review of Scientific Instruments **76** (2005) 19.
 19. P. Patimisco, G. Scamarcio, F. K. Tittel, Vincenzo Spagnolo: Sensors **14**, **4** (2014) 6165-6206.
 20. M. Mordmüller, M. Köhring, W. Schade, U. Willer: Applied Physics B **119** (2015) 111-118.